

HOSTED BY



Contents lists available at ScienceDirect

## Saudi Pharmaceutical Journal

journal homepage: [www.sciencedirect.com](http://www.sciencedirect.com)

Original article

# Piperazine amides with desirable solubility, physicochemical and drug-like properties: Synthesis and evaluation of the anti-*Trypanosoma cruzi* activity

 Marina T. Varela<sup>a,b</sup>, Maiara Romanelli<sup>c</sup>, Maiara Amaral<sup>d</sup>, Andre G. Tempone<sup>c,\*</sup>, João Paulo S. Fernandes<sup>b,\*</sup>
<sup>a</sup> Departamento de Medicina, Universidade Federal de São Paulo, Rua Botucatu 740, 04023-062 São Paulo, SP, Brazil

<sup>b</sup> Departamento de Ciências Farmacêuticas, Universidade Federal de São Paulo, Rua São Nicolau 210, 09913-030 Diadema, SP, Brazil

<sup>c</sup> Centre for Parasitology and Mycology, Instituto Adolfo Lutz, Av. Dr. Arnaldo 351, 01246-000 São Paulo, SP, Brazil

<sup>d</sup> Faculdade de Medicina, Universidade de São Paulo, São Paulo 05403-000, Brazil

## ARTICLE INFO

## Article history:

Received 16 March 2023

Accepted 12 May 2023

Available online 19 May 2023

## Keywords:

Antitrypanosoma activity

Drug-likeness

Solubility

SAR study

*Trypanosoma cruzi*

## ABSTRACT

The absence of effective chronic treatment, expansion to non-endemic countries and the significant burden in public health have stimulated the search for novel therapeutic options to treat Chagas disease, a protozoan disease caused by *Trypanosoma cruzi*. Despite current efforts, no new drug candidates were approved in clinical trials in the past five decades. Considering this, our group has focused on the expansion of a series (LINS03) with low micromolar activity against amastigotes, considering the optimization of pharmacokinetic properties through increasing drug-likeness and solubility. In this work, we report a new set of 13 compounds with modifications in both the arylpiperazine and the aromatic region linked by an amide group. Five analogues showed activity against intracellular amastigotes (IC<sub>50</sub> 17.8 to 35.9 μM) and no relevant cytotoxicity to mammalian cells (CC<sub>50</sub> > 200 μM). Principal component analysis (PCA) was performed to identify structural features associated to improved activity. The data revealed that polarity, hydrogen bonding ability and flexibility were key properties that influenced the antiparasitic activity. *In silico* drug-likeness assessments indicated that compounds with the 4-methoxycinnamyl (especially compound **2b**) had the most prominent balance between properties and activity in the series, as confirmed by SAR analysis.

© 2023 The Author(s). Published by Elsevier B.V. on behalf of King Saud University. This is an open access article under the CC BY-NC-ND license (<http://creativecommons.org/licenses/by-nc-nd/4.0/>).

## 1. Introduction

The protozoan infection caused by *Trypanosoma cruzi*, Chagas disease (CD), is a Neglected Tropical Disease (NTD) that affects over 7 million people, mostly in Latin America (WHO, 2021). However, transmission through contaminated food ingestion, transfusion of infected blood and organ transplantation played the role to spread the disease to non-endemic regions, such as North America, Europe and Asia (Justiz Vaillant and Sticco, 2022; Shikanai-Yasuda and Carvalho, 2012). The human infective forms are the trypomastigotes, transmitted by the insect vector with main importance in the acute phase of the disease, while amastigotes are intracellular forms responsible for parasite replication and persistence of the disease. The current approved treatment includes only two nitro-heterocyclic compounds (nifurtimox and benznidazole), that show efficacy during the acute phase but have low efficacy in the chronic disease (Kratz et al., 2018; Morillo et al., 2015). Benznidazole (BZN) is the only available drug in Brazil for more than 50 years, causes severe side effects and requires long treatment period (2 to 3 months), making tolerability, management and patient compliance difficult to achieve (Castro et al., 2006). These drawbacks emphasise the current need for more efficacious and safer therapies, with particular selectivity towards the amastigote form, the most relevant during the chronic infection.

Drug discovery for CD is often based on phenotypic screening of compounds, using free trypomastigotes or amastigotes in infected mammalian cells (Kratz, 2019). The intracellular location of the parasites in the phenotypic model also provides useful information regarding selectivity and mammalian cytotoxicity, as the parasite needs a living cell to replicate (Aulner et al., 2019; Mansoldo et al., 2020). Furthermore, since the compounds must permeate through the host cell and afterwards into the parasitic cells to exert activity, cellular-based assays provide an indirect assessment of membrane permeability properties of the active compounds

Drug discovery for CD is often based on phenotypic screening of compounds, using free trypomastigotes or amastigotes in infected mammalian cells (Kratz, 2019). The intracellular location of the parasites in the phenotypic model also provides useful information regarding selectivity and mammalian cytotoxicity, as the parasite needs a living cell to replicate (Aulner et al., 2019; Mansoldo et al., 2020). Furthermore, since the compounds must permeate through the host cell and afterwards into the parasitic cells to exert activity, cellular-based assays provide an indirect assessment of membrane permeability properties of the active compounds

\* Corresponding authors.

 E-mail addresses: [andre.tempone@ial.sp.gov.br](mailto:andre.tempone@ial.sp.gov.br) (A.G. Tempone), [joao.fernandes@unifesp.br](mailto:joao.fernandes@unifesp.br) (J.P.S. Fernandes).

(Gilbert, 2013). LINSO3 series has been under expansion in our group, with some promising results already reported against the amastigotes ( $IC_{50} < 10 \mu M$ ) (Varela et al., 2022, 2018). Further molecular modifications were made to achieve better balance between physicochemical properties and activity. Since piperazine group is a privileged structure in drug design and frequently increases water solubility along with tuned lipophilicity, we designed a set of piperazine-containing molecules to improve antiparasitic activity allied to better pharmacokinetic profile. This first set of these piperazine amides showed antiparasitic activity with improved selectivity towards the parasite (Varela et al., 2022), being compounds **1** and **2** (Fig. 1) highlighted as the most promising analogues with noteworthy lipophilic ligand efficiency and drug-likeness properties. However, these compounds present the catechol moiety that may present biological instability and therefore were selected as prototypes for further structural modification. In this work, we reported a new set of compounds (**1a-g** and **2a-f**, Fig. 1) taking advantage of the available SAR data to overcome these limitations (Varela et al., 2018). The design approach included the maintenance of the piperazine amide motif, with the benzoyl (series **1**) or cinnamoyl (series **2**) moiety linked to the piperazine, with further exploration of substituents in the aromatic and piperazine sides. This helped to better understand the hydrogen bonding and electronic effect contributions on the aromatic side, as well as the role of ionization and flexibility in the piperazine side. These concepts are depicted in Fig. 1.

## 2. Materials and methods

### 2.1. Chemicals

The chemicals were acquired from Sigma-Aldrich Co. in adequate purity to use in the synthetic procedures. The obtained compounds were characterized through  $^1H$  and  $^{13}C$  NMR spectroscopy in a Bruker Advance 300 spectrometer, operating at 300 and 75 MHz frequency, respectively, using TMS as internal standard and the chemical shifts ( $\delta$ ) are presented in ppm.

### 2.2. General procedure for the preparation of aryl piperazine derivatives

Amides were prepared by reacting the adequate benzoic (**1a-g**) or cinnamic (**2a-f**) acids with the desired phenyl or benzyl piperazines (Scheme 1). Briefly, 1.1 mmol of the carboxylic acids were dissolved in dichloromethane (DCM) or dimethylformamide (DMF) followed by addition of 1.1 mmol of *N*-(3-dimethylaminopropyl)-*N'*-ethylcarbodiimide hydrochloride (EDC.HCl) and 1-hydroxybenzotriazole hydrate (HOBT·xH<sub>2</sub>O). The activation reaction was allowed for 1 h, when 1 mmol of the substituted piperazine was added in the reaction vessel. The reaction mixture

was stirred at room temperature for 24 h and afterwards distilled water was added. The organic layer was washed sequentially with distilled water, sodium bicarbonate solution and brine, and dried with anhydrous sodium sulphate and evaporated. Crude material was purified through column chromatography, using silica gel and hexane:ethyl acetate mixtures as eluent.

### 2.3. Anti-trypomastigote assay

*T. cruzi* trypomastigotes (Y strain) were added ( $1 \times 10^6$  cells/well) to 96-well microplates and incubated in RPMI 1640 medium for 24 h at 37 °C (5% CO<sub>2</sub> humidified incubator) with different concentrations of the test compounds (150 to 1.1  $\mu M$ , 1:2 dilution). Subsequently, resazurin (0.011% v/v) was added for 24 h to assess the parasite viability. The analysis was performed using a spectrophotometer (FilterMax F5, Molecular Devices) at 570 nm. The 50% inhibitory concentration ( $IC_{50}$ ) values were estimated by non-linear regression analysis, using untreated trypomastigotes as 100% viability. DMSO was added at final concentration of 0.5% (v/v) per well and an internal control was used to confirm the lack of toxicity of the solvent for the parasites at this concentration. BZN was used as reference drug (Romanelli et al., 2022).

### 2.4. Anti-amastigote assay

The  $IC_{50}$  values for amastigote forms of *T. cruzi* were determined as follows. Peritoneal macrophages were collected from BALB/c mice and seeded ( $1 \times 10^5$ ) in 16-well chamber slides (NUNC, Thermo Fisher Scientific). These macrophages were infected with *T. cruzi* trypomastigotes (1:10 macrophage-parasite ratio) during 2 h. After washing out the extracellular parasites with medium, the infected cells were treated with the test compounds in different concentrations (60 to 0.93  $\mu M$ , 1:2 dilution) at 37 °C in a 5% CO<sub>2</sub> humidified incubator for 48 h. The cells were transferred to slides and were then fixed with MeOH, stained with Giemsa and observed under a light microscope (EVOS M500, Thermo). Investigation of compounds' cytotoxicity to macrophages was verified at the highest concentration (i.e. 60  $\mu M$ ) through macrophages' counts, and only compounds that did not caused relevant cytotoxicity at this concentration were considered in the assay. The infection index was obtained in 200 macrophages and used to calculate the  $IC_{50}$  through non-linear regression. DMSO was added at final concentration of 0.5% (v/v) per well and an internal control was used to confirm the lack of toxicity of the solvent for the parasites at this concentration. BZN was used as the reference drug (Romanelli et al., 2022).

### 2.5. Cytotoxicity against mammalian cells

To determine the 50% cytotoxic concentration ( $CC_{50}$ ), fibroblasts NCTC cells (clone 929) were seeded ( $6 \times 10^4$  cells/well) in 96-well

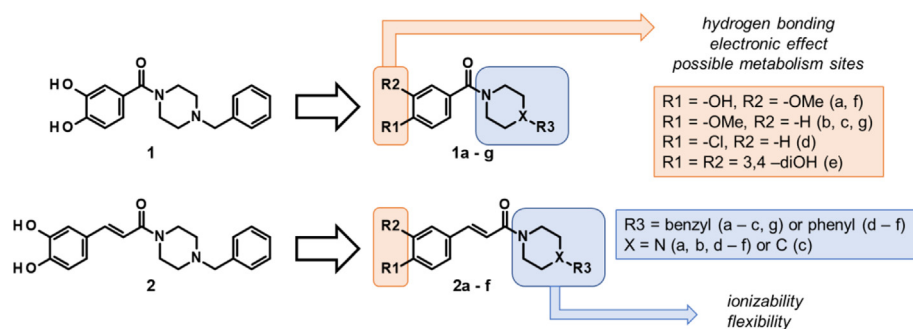
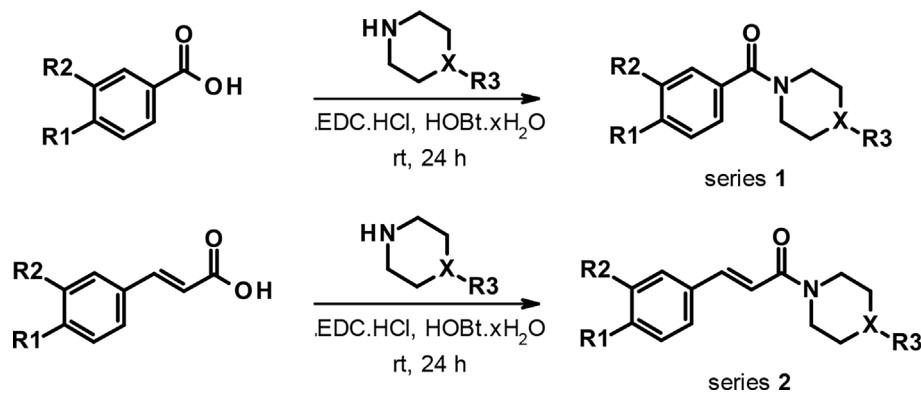


Fig. 1. Previously reported benzylpiperazine amides (**1** and **2**) and novel piperazine amide derivatives **1a-g** and **2a-f**.



**Scheme 1.** General synthetic method for the preparation of the compounds.

microplates and incubated with the compounds (200 to 1.5  $\mu\text{M}$ , 1:2 dilution) for 48 h, at 37  $^{\circ}\text{C}$  in a 5%  $\text{CO}_2$  humidified incubator. The cell viability was spectrophotometrically determined by the MTT method (Tada et al., 1986) using a spectrophotometer at 570 nm (FilterMax F5, Molecular Devices, USA). DMSO was added at final concentration of 0.5% (v/v) per well and an internal control was used to confirm the lack of toxicity of the solvent for the parasites at this concentration. The selectivity index (SI) was determined by the ratio between  $\text{CC}_{50}$  in NCTC and the  $\text{IC}_{50}$  values (Amaral et al., 2019).

The determination of the  $\text{CC}_{50}$  and  $\text{IC}_{50}$  values was obtained from sigmoid dose–response curves, using Graph Pad Prism 6.0 software. All the assays were replicated twice and samples tested in duplicates (Amaral et al., 2019).

## 2.6. Calculation of physicochemical properties

Lipophilicity (cLogP), distribution coefficient ( $\text{LogD}_{7.4}$ ), aqueous solubility at pH 7.4 ( $\text{LogS}_{7.4}$ ) and other structural descriptors used in the chemometric analysis were calculated using MarvinSketch 20.21 (ChemAxon, Inc.) in the default settings. Drug-likeness score and overall drug score were calculated using OSIRIS Property Explorer (organic-chemistry.org), using an algorithm that combines structural features and physicochemical properties into values that describe the drug-likeness of a given compound.

## 2.7. Statistical SAR analysis

The principal component analysis (PCA) was done using values of those descriptors. The values were autoscaled prior to analysis using the software PAST 4.03 (Hammer et al., 2001). Initial descriptor selection was done by visual inspection of raw data. For those, the PCA was carried out several times and five descriptors with higher loading values in the PC1 and PC2 (polarizability, dipole moment [ $\mu$ ], fraction of  $\text{sp}^3$ -hybridized carbons [ $\text{Fsp}^3$ ], hydrogen bond donor [HBD] and acceptor [HBA] counts) were kept in the model, allowing to discriminate between active and inactive compounds.

## 2.8. Drug-likeness analysis

Drug-like properties of solubility (ESOL class), gastrointestinal (GI) absorption, P-glycoprotein (P-gp) substrate, Lipinski's Rule of Five violations and PAINS alerts were calculated for the active compounds using the SwissADME on-line platform (Daina et al., 2017).

## 3. Results

### 3.1. Synthesis of the compounds

The compounds were successfully prepared according to the described methodology (Scheme 1), with adequate yields to the biological evaluation. Characterization and obtained yields are described below.

#### 3.1.1. (4-Benzylpiperazin-1-yl)(4-hydroxy-3-methoxyphenyl)methanone (**1a**)

Reaction between vanillic acid and 1-benzylpiperazine yielded 22% of a yellow oil.  $^1\text{H}$  NMR (300 MHz,  $\text{DMSO}-d_6$ ,  $\delta$  = ppm, TMS) 2.37 (br s, 4H), 3.50 (br s, 6H), 3.77 (s, 3H), 6.73–6.86 (m, 2H), 6.93 (s, 1H), 7.20–7.39 (m, 5H), 9.40 (br s, 1H).  $^{13}\text{C}$  NMR (75 MHz,  $\text{CDCl}_3$ ,  $\delta$  = ppm, TMS) 53.04, 55.99, 62.88, 110.70, 114.00, 120.75, 127.27, 127.37, 128.36, 129.26, 137.28, 146.70, 147.29, 170.35.

#### 3.1.2. (4-Benzylpiperazin-1-yl)(4-methoxyphenyl)methanone (**1b**)

Reaction between 4-methoxybenzoic acid and 1-benzylpiperazine yielded 47% of a yellow oil.  $^1\text{H}$  NMR (300 MHz,  $\text{CDCl}_3$ ,  $\delta$  = ppm, TMS) 2.48 (br s, 4H), 3.56 (s, 2H), 3.64 (br s, 4H), 3.82 (s, 3H), 6.90 (d,  $J$  = 8.8 Hz, 2H), 7.26–7.35 (m, 5H), 7.38 (d,  $J$  = 8.8 Hz, 2H).  $^{13}\text{C}$  NMR (75 MHz,  $\text{CDCl}_3$ ,  $\delta$  = ppm, TMS) 53.08, 55.35, 62.93, 113.68, 127.30, 127.92, 128.34, 129.14, 129.17, 137.55, 160.72, 170.27.

#### 3.1.3. 4-Benzyl-1-(4-methoxybenzoyl)piperidine (**1c**)

Reaction between 4-methoxybenzoic acid and 1-benzylpiperidine yielded 66% of a white solid (mp 63–65  $^{\circ}\text{C}$ ).  $^1\text{H}$  NMR (300 MHz,  $\text{CDCl}_3$ ,  $\delta$  = ppm, TMS) 1.07–1.53 (m, 3H), 1.54–1.92 (m, 4H), 2.57 (d,  $J$  = 7.0 Hz, 2H), 2.82 (br s, 2H), 3.82 (s, 3H), 6.90 (dt,  $J$  = 8.8, 2.3 Hz, 2H), 7.10–7.33 (m, 5H), 7.36 (dt,  $J$  = 8.8, 2.3 Hz, 2H).  $^{13}\text{C}$  NMR (75 MHz,  $\text{CDCl}_3$ ,  $\delta$  = ppm, TMS) 32.26, 38.42, 43.05, 55.34, 113.63, 126.06, 128.32, 128.48, 128.93, 129.09, 139.99, 160.58, 170.32.

#### 3.1.4. (3,4-dihydroxyphenyl)-(4-phenylpiperazin-1-yl)methanone (**1d**)

Reaction between 3,4-dihydroxybenzoic acid and 1-phenylpiperazine yielded 10% of a light brown solid (mp 127–129  $^{\circ}\text{C}$ ).  $^1\text{H}$  NMR (300 MHz,  $\text{DMSO}-d_6$ ,  $\delta$  = ppm, TMS) 3.91 (br s, 4H), 4.22 (br s, 4H), 6.65–6.86 (m, 5H), 6.90–7.05 (m, 1H), 7.15–7.30 (m, 2H), 9.10–9.50 (m, 2H).  $^{13}\text{C}$  NMR (75 MHz,  $\text{DMSO}-d_6$ ,  $\delta$  = ppm, TMS) 49.08, 115.55, 115.59, 116.36, 119.49, 119.82, 126.81, 129.45, 145.42, 147.45, 151.30, 169.78.

### 3.1.5. (4-hydroxy-3-methoxyphenyl)(4-phenylpiperazin-1-yl)methanone (**1e**)

Reaction between vanillic acid and 1-phenylpiperazine yielded 37% of a white solid (mp 168–170 °C). <sup>1</sup>H NMR (300 MHz, CD<sub>3</sub>OD, δ = ppm, TMS) 3.20 (br s, 4H), 3.80 (br s, 4H), 3.92 (s, 3H), 5.85 (br s, 1H), 6.86–7.00 (m, 5H), 7.27–7.33 (m, 3H). <sup>13</sup>C NMR (75 MHz, CDCl<sub>3</sub>, δ = ppm, TMS) 49.79, 56.05, 110.69, 113.95, 116.71, 120.62, 120.84, 127.19, 129.27, 146.68, 147.35, 150.98, 170.43.

### 3.1.6. (4-methoxyphenyl)(4-phenylpiperazin-1-yl)methanone (**1f**)

Reaction between 4-methoxybenzoic acid and 1-phenylpiperazine yielded 35% of a white solid (mp 117–119 °C). <sup>1</sup>H NMR (300 MHz, CDCl<sub>3</sub>, δ = ppm, TMS) 3.19 (br s, 4H), 3.50–4.15 (m, 7H), 6.80–7.05 (m, 5H), 7.20–7.35 (m, 2H), 7.43 (d, J = 8.3 Hz, 2H). <sup>13</sup>C NMR (75 MHz, CDCl<sub>3</sub>, δ = ppm, TMS) 49.76, 55.39, 113.79, 116.71, 120.57, 127.67, 129.26, 151.02, 160.90, 170.40.

### 3.1.7. 1-benzyl-4-(4-chlorobenzoyl)piperazine (**1g**)

Reaction between 4-chlorobenzoic acid and 1-benzylpiperazine yielded 86% of a white solid (mp 98–100 °C). <sup>1</sup>H NMR (300 MHz, CDCl<sub>3</sub>, δ = ppm, TMS) 2.42 (br s, 2H), 2.51 (br s, 2H), 3.41 (br s, 2H), 3.54 (s, 2H), 3.77 (br s, 2H), 7.24–7.40 (m, 9H). <sup>13</sup>C NMR (75 MHz, CDCl<sub>3</sub>, δ = ppm, TMS) 52.81, 62.88, 127.35, 128.37, 128.63, 128.75, 129.13, 134.18, 135.74, 137.46, 169.21.

### 3.1.8. (2E)-1-(4-benzylpiperazin-1-yl)-3-(4-hydroxy-3-methoxyphenyl)prop-2-en-1-one (**2a**)

Reaction between ferulic acid and 1-benzylpiperazine yielded 32% of a yellow solid (mp 138–140 °C). <sup>1</sup>H NMR (300 MHz, CDCl<sub>3</sub>, δ = ppm, TMS) 2.42–2.54 (m, 4H), 3.54 (s, 2H), 3.70 (br s, 4H), 3.92 (s, 3H), 6.70 (d, J = 15.3 Hz, 1H), 6.90 (d, J = 8.2 Hz, 1H), 6.98 (d, J = 1.7 Hz, 1H), 7.09 (dd, J = 8.2, 1.7 Hz, 1H), 7.28–7.35 (m, 5H), 7.60 (d, J = 15.3 Hz, 1H). <sup>13</sup>C NMR (75 MHz, CDCl<sub>3</sub>, δ = ppm, TMS) 42.21, 55.99, 62.92, 109.84, 114.56, 114.72, 121.87, 127.29, 127.89, 128.35, 129.16, 137.63, 142.87, 146.67, 147.29, 165.64.

### 3.1.9. (2E)-1-(4-benzylpiperazin-1-yl)-3-(4-methoxyphenyl)prop-2-en-1-one (**2b**)

Reaction between 4-methoxycinnamic acid and 1-benzylpiperazine yielded 82% of a yellow oil. <sup>1</sup>H NMR (300 MHz, CDCl<sub>3</sub>, δ = ppm, TMS) 2.48 (m, 4H), 3.45 (s, 2H), 3.70 (br s, 4H), 3.83 (s, 3H), 6.73 (d, J = 15.4 Hz, 1H), 6.89 (d, J = 8.7 Hz, 2H), 7.27–7.35 (m, 5H), 7.46 (d, J = 8.7 Hz, 2H), 7.63 (d, J = 15.4 Hz, 1H). <sup>13</sup>C NMR (75 MHz, CDCl<sub>3</sub>, δ = ppm, TMS) 52.84, 55.37, 62.90, 114.22, 114.59, 127.31, 128.05, 128.36, 129.18, 129.31, 137.58, 142.46, 160.83, 165.71.

### 3.1.10. (2E)-1-(1-benzylpiperidin-4-yl)-3-(4-methoxyphenyl)prop-2-en-1-one (**2c**)

Reaction between 4-methoxycinnamic acid and 1-benzylpiperidine yielded 45% of a white solid (mp 84–86 °C). <sup>1</sup>H NMR (300 MHz, CDCl<sub>3</sub>, δ = ppm, TMS) 1.14–1.35 (m, 2H), 1.67–1.91 (m, 3H), 2.56 (br s, 3H), 3.05 (br s, 1H), 3.83 (s, 3H), 4.08 (br s, 1H), 4.70 (br s, 1H), 6.75 (d, J = 15.4 Hz, 1H), 6.88 (d, J = 8.7 Hz, 2H), 7.11–7.35 (m, 5H), 7.46 (d, J = 8.6 Hz, 2H), 7.62 (d, J = 15.3 Hz, 1H). <sup>13</sup>C NMR (75 MHz, CDCl<sub>3</sub>, δ = ppm, TMS) 38.39, 42.99, 55.36, 114.19, 115.11, 126.06, 128.18, 128.32, 129.11, 129.25, 140.00, 142.09, 160.73, 165.69.

### 3.1.11. (2E)-3-(3,4-dihydroxyphenyl)-1-(4-phenylpiperazin-1-yl)prop-2-en-1-one (**2d**)

Reaction between caffeic acid and 1-phenylpiperazine yielded 23% of light brown solid (mp 168–170 °C). <sup>1</sup>H NMR (300 MHz, CD<sub>3</sub>OD, δ = ppm, TMS) 3.27 (br s, 4H), 3.90 (br s, 4H), 6.78 (d, J = 8.2 Hz, 1H), 6.92 (d, J = 15.3 Hz, 2H), 6.98–7.02 (m, 1H), 7.05–7.10 (m, 3H),

7.30 (t, J = 8.4 Hz, 2H), 7.50 (d, J = 15.3 Hz, 1H). <sup>13</sup>C NMR (75 MHz, CD<sub>3</sub>OD, δ = ppm, TMS) 112.89, 114.03, 115.08, 120.96, 127.10, 128.87, 143.87, 145.33, 147.61, 166.90.

### 3.1.12. (2E)-3-(4-hydroxy-3-methoxyphenyl)-1-(4-phenylpiperazin-1-yl)prop-2-en-1-one (**2e**)

Reaction between ferulic acid and 1-phenylpiperazine: yielded 28% of a yellow solid (mp 168–170 °C). <sup>1</sup>H NMR (300 MHz, CD<sub>3</sub>OD, δ = ppm, TMS) 3.16 (br s, 4H), 3.72 (br s, 4H), 3.84 (s, 3H), 6.74–6.86 (m, 2H), 6.99 (d, J = 7.9 Hz, 2H), 7.04–7.17 (m, 2H), 7.18–7.31 (m, 2H), 7.32–7.38 (m, 1H), 7.45 (d, J = 15.3 Hz, 1H), 9.44 (br s, 1H). <sup>13</sup>C NMR (75 MHz, CDCl<sub>3</sub>, δ = ppm, TMS) 49.73, 56.02, 109.99, 114.19, 114.83, 166.66, 120.58, 121.98, 127.74, 129.29, 143.41, 146.77, 147.50, 150.94, 165.87.

### 3.1.13. (2E)-3-(4-methoxyphenyl)-1-(4-phenylpiperazin-1-yl)prop-2-en-1-one (**2f**)

Reaction between 4-methoxycinnamic acid and 1-phenylpiperazine yielded 36% of a white solid (mp 156–158 °C). <sup>1</sup>H NMR (300 MHz, CDCl<sub>3</sub>, δ = ppm, TMS) 3.01–3.26 (m, 4H), 3.65–4.00 (m, 7H), 6.72 (d, J = 15.3 Hz, 1H), 6.77–6.94 (m, 5H), 7.15–7.28 (m, 2H), 7.42 (d, J = 8.6 Hz, 2H), 7.61 (d, J = 15.3 Hz, 1H). <sup>13</sup>C NMR (75 MHz, CDCl<sub>3</sub>, δ = ppm, TMS) 49.65, 55.39, 114.27, 114.35, 116.63, 120.51, 127.96, 129.28, 129.39, 142.82, 150.97, 160.94, 165.80.

## 3.2. Activity against *T. cruzi* and cytotoxicity assessment

Results from the evaluation of the activity against both trypomastigote and amastigote forms of *T. cruzi*, as well as the assessment of the cytotoxicity towards mammalian cells are presented in [Table 1](#).

## 3.3. Calculation of molecular descriptors

The five selected descriptors for SAR studies are presented in [Table 2](#) with respective values. These values were autoscaled prior to their use in the PCA procedure.

## 3.4. Pca

The results from PCA indicated that 71% of the total variance was explained by the first two PCs (PC1 39%; PC2 32%). PC1 was comprised mainly by the descriptors Fsp3, HBA and HBD whereas PC2 was mainly represented by electronic descriptors of polarizability and dipole moment. Loading values for the descriptors in each PC are depicted in [Table 3](#). The distribution plot of the compounds in relation to PC1 and PC2 values is presented in [Fig. 2](#). Active compounds were clustered into two groups, A and B, of mono- and di-substituted analogues, respectively, as indicated in [Fig. 2](#).

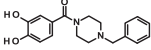
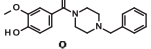
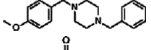
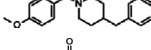
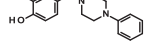
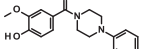
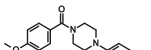
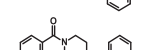
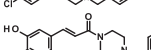
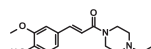
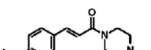
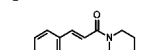
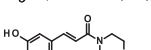

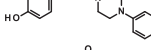
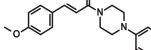
## 3.5. Drug-likeness assessment

The assessment of the compounds on the SwissADME on-line platform resulted in the data presented in [Table 4](#). The compounds presented high predicted solubility, adequate permeation through GI tract and general adequate pharmacokinetic and drug-like profile.



**Table 1**

Efficacy data (IC<sub>50</sub>) determined for *T. cruzi* trypomastigotes (**T.c.T**) and amastigotes (**T.c.A**) and cytotoxicity (CC<sub>50</sub>) determined for mammalian NCTC cells (clone L929). Values for LogD<sub>7,4</sub> were calculated in MarvinSketch 20.21.

Entry	Structure	IC <sub>50</sub> (μM ± SD)		NCTC	SI	LogD <sub>7,4</sub>	LogS <sub>7,4</sub>
		T.c.T	T.c.A				
<b>1<sup>#</sup></b>		42.5 ± 8.9	28.2 ± 3.8	>200	>7.1	2.11	-2.44
<b>1a</b>		>150	35.9 ± 3.4	>200	>5.6	2.27	-2.86
<b>1b</b>		>150	>60	>200	ND	2.58	-3.29
<b>1c</b>		65.3 ± 2.3	>60	>200	ND	3.83	-4.55
<b>1d</b>		>150	34.8 ± 9.0	>200	>5.7	2.36	-3.16
<b>1e</b>		>150	>60	>200	ND	2.54	-3.60
<b>1f</b>		>150	>60	>200	ND	2.85	-4.04
<b>1g</b>		>150	>60	>200	ND	3.61	-4.77
<b>2<sup>#</sup></b>		46.4 ± 0.9	13.0 ± 7.1	>200	>15.4	2.56	-2.93
<b>2a</b>		>150	>60	>200	ND	2.71	-3.33
<b>2b</b>		>150	28.6 ± 7.7	>200	>7	3.02	-3.77
<b>2c</b>		>150	17.8 ± 9.0	>200	>11.2	4.33	-5.08
<b>2d</b>		19.5 ± 7.4	20.4 ± 3.7	57.2 ± 2.0	2.8	2.90	-3.73
<b>2e</b>		>150	>60	>200	ND	3.05	-4.14
<b>2f</b>		>150	>60	>200	ND	3.36	-4.58
<b>BZN</b>		12.3 ± 3.3	5 ± 1.5	>200	>40	-	-

<sup>#</sup> Varela et al., 2022. NA: not active. DP: standard deviation BZN: benznidazole. SI: Selective Index, given by the ratio between CC<sub>50</sub> and IC<sub>50</sub> (amastigote - TCA).

## 4. Discussion

### 4.1. Antitrypanosomal activity and cytotoxicity

The optimization of LINSO3 series of compounds was done considering to improve the activity/selectivity profile of the compounds allied to adequate physicochemical properties for oral bioavailability. This strategy in early drug discovery allows initial selection of promising compounds with balanced predicted pharmacodynamic and pharmacokinetic profiles (Shi and Zha, 2019; Sohlenius-Sternbeck et al., 2016). The piperazine amide derivatives **1** and **2** were previously reported as promising trypanocidal candidates in the LINSO3 series, with improved activity and physicochemical properties from the previous set (Varela et al., 2022), suggesting the maintenance of this motif in the structure. Although the catechol ring was associated with the greatest improvements in both activity and hydrosolubility of previously reported compounds, it can also be associated with high metabolic instability and potential toxicity related to quinone formation (Cavaliere et al., 2002; Zhu, 2002). Therefore, the compounds herein reported (Table 1) were designed by mainly modifying the catechol motif to

guaiacol (3-methoxy-4-hydroxy) or 4-methoxybenzene analogues (Varela et al., 2019) to overcome these issues. These patterns were present in other amides of the LINSO3 series and preliminary stability data indicated that these substructures were less susceptible to oxidative metabolism than corresponding catechol-containing compounds (data not shown).

The obtained activity data (Table 1) provided some useful SAR information about this series. For instance, the 3-methoxy (**1a**) analogue of compound **1** maintained the activity against the amastigotes but lost the anti-trypomastigote activity. Modification of the benzyl group to phenyl mostly led to inactive compounds, except for compound **1d**. Compound **1c** was the only derivative in the benzoyl amide set to show moderate activity against trypomastigotes (IC<sub>50</sub> 65.3 μM).

On the other hand, cinnamic acid derivatives were more promising, highlighting the importance of the benzylidene substructure to enhance the anti-*T. cruzi* activity. Comparable anti-amastigote activity was observed between 4-methoxy derivatives **2b** and **2c** (IC<sub>50</sub> 28.6 μM and 17.9 μM, respectively) to the catechol prototype **2** (IC<sub>50</sub> 13.0 μM), suggesting that hydroxy groups in the aromatic ring are not essential to the activity. The comparable

**Table 2**  
Molecular descriptors calculated in MarvinSketch 20.21 used for the principal component analysis.

Entry	Structure	Polarizability (Å <sup>3</sup> )	μ (Debye)	Fsp3	HBA	HBD
1 <sup>#</sup>		33.79	8.31	0.44	5	2
1a		35.71	8.52	0.47	5	1
1b		28.39	10.03	0.42	4	0
1c		35.55	9.72	0.40	3	0
1d		32.02	7.78	0.35	5	2
1e		33.72	9.29	0.39	5	1
1f		33.34	8.93	0.33	4	0
1g		34.25	5.05	0.33	3	0
2 <sup>#</sup>		37.45	10.83	0.40	5	2
2a		39.43	12.07	0.43	5	1
2b		38.73	12.57	0.38	4	0
2c		39.14	11.78	0.36	3	0
2d		35.63	9.94	0.32	5	2
2e		37.65	11.14	0.35	5	1
2f		36.89	12.02	0.30	4	0

Fsp3 = number of sp<sup>3</sup> hybridized carbons/total number of carbons.

**Table 3**  
Loading values for the physicochemical descriptors in the 2 principal components.

Component	Polarizability	μ	Fsp3	HBA	HBD
PC1	-0.151	-0.143	0.341	0.646	0.649
PC2	0.682	0.694	0.027	0.211	0.087

activity of **2b** and **2c** indicates that the basic nitrogen atom is also not essential to the antiparasitic activity, but it provides advantage in the solubility for compound **2b** (1.3-log unit increase in Log<sub>S<sub>7.4</sub></sub> value) with desirable lipophilicity (Log<sub>D<sub>7.4</sub></sub> 3.05) over the neutral analogue **2c**. Catecholic derivative **2d** was the only compound in the set to show trypanocidal activity against both forms of the parasite; however, the cytotoxicity to mammalian cells increased accordingly, suggesting an unspecific toxic activity not observed for other compounds. This profile may be related to the presence of the phenylpiperazine moiety, since the benzylpiperazine counterpart **2** did not show important cytotoxic activity. Additionally, most of the active compounds (**1**, **1a**, **2** and **2b**) are benzylpiperazines, suggesting that the presence of a basic nitrogen and/or higher flexibility may increase the antiparasitic activity with higher selectivity.

Another important criterion during evaluation of hit compounds is the selectivity index (SI) measured as the ratio mam-

malian cytotoxicity/activity against amastigotes. The Drug for Neglected Diseases *initiative* (DNDi) suggests a hit selection criterion as IC<sub>50</sub> value < 10 μM (against amastigotes) and selectivity index > 10 (Don and Ioset, 2014; Katsuno et al., 2015). Except for compound **2d**, the tested compounds showed promising profile, with no important cytotoxicity to mammalian cells up to 200 μM. With these regard, compounds **2b** and **2c** must be highlighted as the most promising and selective (SI > 10).

#### 4.2. Statistical SAR analysis

Previously studied compounds showed a good correlation between active compounds and hydrosolubility, described by Log<sub>D<sub>7.4</sub></sub> and Log<sub>S<sub>7.4</sub></sub> values (Varela et al., 2022). Although most of the active compounds had balanced lipophilicity and solubility properties, this relationship was not clearly observed in this series. Compounds **2b** (Log<sub>D<sub>7.4</sub></sub> 3.02 and Log<sub>S<sub>7.4</sub></sub>-3.77) and **2c** (Log<sub>D<sub>7.4</sub></sub>

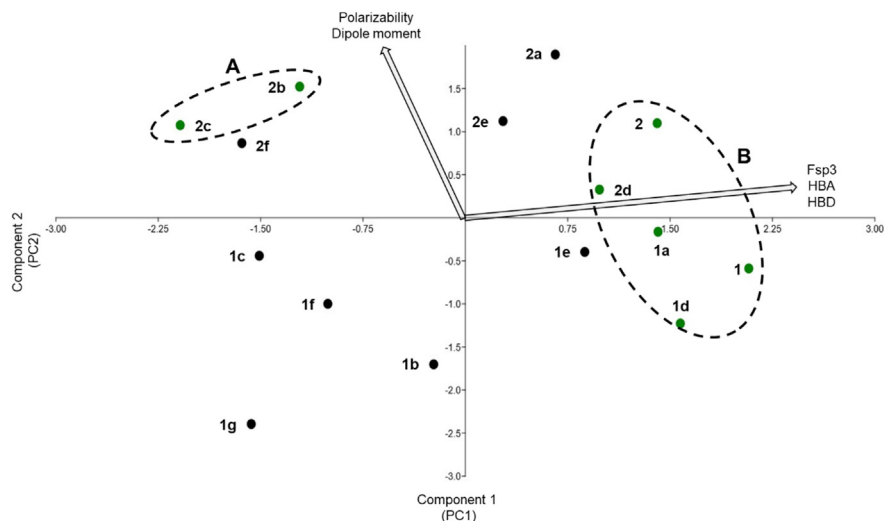


Fig. 2. Distribution plot of compounds 1–1 g and 2-2f according to the PCA. Green: active compounds. Black: inactive compounds.

Table 4

Results of predicted pharmacokinetic and drug-like properties obtained from SwissADME platform.

Cpd	ESOL class	GI Absorption	P-gp substrate	Lipinski's Ro5 violations	Drug-likeness
1	Soluble	High	Yes	0	Yes
1a	Soluble	High	No	0	Yes
1d	Soluble	High	Yes	0	Yes
2	Soluble	High	Yes	0	Yes
2b	Soluble	High	No	0	Yes
2c	Moderate	High	No	0	Yes
2d	Soluble	High	No	0	Yes

4.33 and  $\text{LogS}_{7.4}$  5.08) are less hydrosoluble than prototype **2** ( $\text{LogD}_{7.4}$  2.56 and  $\text{LogS}_{7.4}$  -2.93) but similar activity against the parasite was obtained. The discrepancy in the observed activity between benzoyl and cinnamyl series suggests that these hydrosolubility/lipophilicity descriptors were not enough to explain the biological activity. Therefore, other structural and physicochemical properties should be studied through additional descriptors to provide a better understanding of the SAR.

Principal component analysis (PCA) has been used to identify the roles of molecular descriptors by distributing the compounds into subsets. By converting the original variables to orthogonal principal components (PCs) that describe similar information, the obtained two-dimensional plot allows the visual analysis of these data (Abdi and Williams, 2010). In the context of this work, PCA allowed visual separation between active and inactive compounds in clusters given by the descriptors that composes each PC (Table 3), and therefore such descriptors can be correlated to the activity (Guo, 2017).

Several structural, electronic, topological and geometrical molecular descriptors were calculated and used in the analysis. After visual inspection from several PCA runs, descriptors with higher loading scores were prioritized based on the clustering of compounds. The five selected descriptors, polarizability, dipole moment ( $\mu$ ), fraction of  $\text{sp}^3$ -hybridized carbons (Fsp3) and hydrogen bond acceptors (HBA) and donors (HBD) (Table 2), resulted in the best clustering of active and inactive compounds. These descriptors are also correlated to lipophilicity and solubility, since they describe the molecule in terms of polarity and flexibility.

It can be noted in Fig. 2 that cinnamoyl amide derivatives (series **2**) had positive values for PC2 (y-axis) while benzoyl amides (series **1**) had negative PC2 values, indicating that derivatives of the subset **2** are more polar than the subset **1**. This suggests that

by maintaining the electronic conjugation between aromatic ring and carbonyl group, the vinylic spacer led to different electron density in the molecules and therefore higher polarity for compounds from series **2**. Nevertheless, mono-substituted compounds were distributed on the negative left-side of the x-axis (PC1), while di-substituted compounds were on the positive side, describing the increase in the flexibility and hydrogen-bonding ability given by the substitution pattern in the aromatic ring. The obtained clustering suggests that 4-substituted compounds depend on different molecular characteristics from the 3,4-disubstituted to present high activity. This suggests that presence of the substituent in the 3-position may lead to specific molecular effects that directly affect activity.

4-Substituted analogues in the aromatic ring **2b** and **2c** are in the top-left quadrant, where negative values for PC1 and positive values for PC2 are found. This means that these compounds present high values for polarizability and dipole moment associated with lower values for Fsp3, HBA and HBD. Considering that compounds **2b** and **2c** are active compounds while the benzoyl amides counterparts **1b** and **2c** are inactive, this analysis suggests that vinylic spacer modified the polarizability and dipole moment in a way to play the role on activity. Polarizability refers to the charge distribution to an applied force field (i.e. induced dipole moment), whereas the dipole moment relates to the net charge distribution in the molecule (Das et al., 2021; Tandon et al., 2021).

The active 3,4-substituted analogues were clustered on the right side of the distribution plot, suggesting that increased activity is associated with hydrogen-bonding ability. In fact, active compounds in cluster B (except **1a**) are catechols, denoting the positive effect of the number of HBD groups on activity. Compounds in cluster B have five HBA and two HBD groups, except for **1a**. On the other hand, the inactive compounds **2a** and **2e** have the highest

values for polarizability and dipole moment among the 3,4-substituted analogues, suggesting that excessive polarity may reduce the antiparasitic activity indeed.

This SAR analysis provided helpful insight to understand which molecular features are associated to the biological activity of compounds, as previously discussed. The electronic descriptors were important to separate between active and inactive compounds, particularly by describing modifications of the aromatic region of the amide moiety. For the 3-substituted analogues, higher polarizability and dipole moment values increased antiparasitic activity, whereas for 3,4-disubstituted analogues activity seems to be correlated to the presence of the catechol (with increased HBD count).

#### 4.3. Drug-likeness assessment

Although the obtained compounds possess similar activity against the amastigotes to the prototypes **1** and **2**, the drug-likeness was considerably improved in this new series. Catechol motif is frequently associated to chemical or enzymatic instability due to its susceptibility to oxidation reactions, that involve the conversion of hydroxy groups to reactive quinones. The proposed modifications in the aromatic moiety improved the drug-likeness of the compounds as suggested by the *in silico* assessment (Table 4), carried out in the SwissADME platform (Daina et al., 2017). This tool enables rapid and reliable predictions of physicochemical, pharmacokinetic and medicinal chemistry descriptors, and therefore has been broadly used for this purpose (Bakchi et al., 2022; Pantaleão et al., 2022).

Catechol analogues **1**, **1d**, and **2** were identified as possible substrates of P-gp, which is associated to efflux of xenobiotics. This may indicate future issues regarding bioavailability and tissue distribution related to catechol structure. Thus, the modification of this motif should be considered an improvement for non-catecholic compounds **2b** and **2c**. Obtained data also suggested that the novel compounds have high GI absorption due to their balanced lipophilicity and hydrosolubility. The compounds had also high predicted solubility, with exception of the analogue **2c** due to the absence of an ionizable group in its structure.

## 5. Conclusions

Given together, the results suggest that 4-methoxycinnamates **2b** and **2c** are the promising compounds with antiparasitic activity and improved drug-likeness. These compounds were statistically equipotent to the prototype **2** but have improved drug-likeness by avoiding the undesired catechol moiety. Compound **2b** should be considered advantageous over **2c** due to its better solubility provided by piperazine motif, and in summary, is a noteworthy prototype for further development as anti-*Trypanosoma* bioactive compound.

## Declaration of Competing Interest

The authors declare that they have no known competing financial interests or personal relationships that could have appeared to influence the work reported in this paper.

## Acknowledgements

The authors are grateful to São Paulo Research Foundation – FAPESP for the financial support to JPSF and AGT (grants n° 2019/24028-8 and 2021/04464-8) and to the scholarship to MTV (grants n° 2018/03918-2 and 2019/14167-0). MTV is also grateful to Coordination for the Improvement of Higher Education Personnel – CAPES (financial code 001). JPSF and AGT acknowledge the

National Council for Scientific and Technological Development – CNPq (grant n° 307829/2021-9).

## References

- Abdi, H., Williams, L.J., 2010. Principal component analysis. Wiley Interdiscip. Rev. Comput. Stat. 2, 433–459. <https://doi.org/10.1002/wics.101>.
- Amaral, M., de Sousa, F.S., Silva, T.A.C., Junior, A.J.G., Taniwaki, N.N., Johns, D.M., Lago, J.H.G., Anderson, E.A., Tempone, A.G., 2019. A semi-synthetic neolignan derivative from dihydrodieugenol B selectively affects the bioenergetic system of *Leishmania infantum* and inhibits cell division. Sci. Rep. 9, 6114. <https://doi.org/10.1038/s41598-019-42273-z>.
- Aulner, N., Danckaert, A., Ihm, J., Shum, D., Shorte, S.L., 2019. Next-Generation phenotypic screening in early drug discovery for infectious diseases. Trends Parasitol. 35, 559–570. <https://doi.org/10.1016/j.pt.2019.05.004>.
- Bakchi, B., Krishna, A.D., Sreecharan, E., Ganesh, V.B.J., Niharika, M., Maharshi, S., Puttagunta, S.B., Sigalapalli, D.K., Bhandare, R.R., Shaik, A.B., 2022. An overview on applications of SwissADME web tool in the design and development of anticancer, antitubercular and antimicrobial agents: a medicinal chemist's perspective. J. Mol. Struct. 1259, <https://doi.org/10.1016/j.molstruc.2022.132712>.
- Castro, J.A., DeMecca, M.M., Bartel, L.C., 2006. Toxic side effects of drugs used to treat Chagas' Disease (American Trypanosomiasis). Hum. Exp. Toxicol. 25, 471–479. <https://doi.org/10.1191/0960327106het6530a>.
- Cavaliere, E.L., Li, K.-M., Balu, N., Saeed, M., Devanesan, P., Higginbotham, S., Zhao, J., Gross, M.L., Rogan, E.G., 2002. Catechol ortho-quinones: the electrophilic compounds that form depurinating DNA adducts and could initiate cancer and other diseases. Carcinogenesis 23, 1071–1077. <https://doi.org/10.1093/carcin/23.6.1071>.
- Daina, A., Michielin, O., Zoete, V., 2017. SwissADME: a free web tool to evaluate pharmacokinetics, drug-likeness and medicinal chemistry friendliness of small molecules. Sci. Rep. 7, 42717. <https://doi.org/10.1038/srep42717>.
- Das, A., Das, A., Banik, B.K., 2021. Influence of dipole moments on the medicinal activities of diverse organic compounds. J. Indian Chem. Soc. 98, <https://doi.org/10.1016/j.jics.2021.100005>.
- Don, R., Ioset, J.-R., 2014. Screening strategies to identify new chemical diversity for drug development to treat kinetoplastid infections. Parasitology 141, 140–146. <https://doi.org/10.1017/S003118201300142X>.
- Gilbert, I.H., 2013. Drug discovery for neglected diseases: molecular target-based and phenotypic approaches. J. Med. Chem. 56, 7719–7726. <https://doi.org/10.1021/jm400362b>.
- Guo, Z., 2017. The modification of natural products for medical use. Acta Pharm. Sin. B 7, 119–136. <https://doi.org/10.1016/j.apsb.2016.06.003>.
- Hammer, Ø., Harper, D.A.T., Ryan, P.D., 2001. PAST: paleontological statistics software package for education and data analysis. Palaeontol. Electron. 4, 9.
- Justiz Vaillant, A.A.J., Sticco, K.L., 2022. Transfusion Transmitted Disease, In: StatPearls, StatPearls Publishing, Treasure Island (FL). PMID: 30860698, Available from: <https://www.ncbi.nlm.nih.gov/books/NBK538427/>.
- Katsuno, K., Burrows, J.N., Duncan, K., van Huijsduijnen, R.H., Kaneko, T., Kita, K., Mowbray, C.E., Schmatz, D., Warner, P., Slingsby, B.T., 2015. Hit and lead criteria in drug discovery for infectious diseases of the developing world. Nat. Rev. Drug Discov. 14, 751–758. <https://doi.org/10.1038/nrd4683>.
- Kratz, J.M., 2019. Drug discovery for chagas disease: a viewpoint. Acta Trop. 198, <https://doi.org/10.1016/j.actatropica.2019.105107>.
- Kratz, J.M., Garcia Bournissen, F., Forsyth, C.J., Sosa-Estani, S., Kratz, J.M., Garcia Bournissen, F., Forsyth, C.J., Sosa-Estani, S., Müller Kratz, J., Garcia Bournissen, F., Forsyth, C.J., Sosa-Estani, S., 2018. Clinical and pharmacological profile of benzimidazole for treatment of Chagas disease. Expert. Rev. Clin. Pharmacol. 11, 943–957. <https://doi.org/10.1080/17512433.2018.1509704>.
- Mansoldo, F.R.P., Carta, F., Angeli, A., Cardoso, V.d.S., Supuran, C.T., Vermelho, A.B., 2020. Chagas Disease: perspectives on the past and present and challenges in drug discovery. Molecules 25, 5483. <https://doi.org/10.3390/molecules25225483>.
- Morillo, C.A., Marin-Neto, J.A., Avezum, A., Sosa-Estani, S., Rassi, A., Rosas, F., Villena, E., Quiroz, R., Bonilla, R., Britto, C., Guhl, F., Velazquez, E., Bonilla, L., Meeks, B., Rao-Melacini, P., Pogue, J., Mattos, A., Lazdins, J., Rassi, A., Connolly, S.J., Yusuf, S., 2015. Randomized trial of benzimidazole for chronic Chagas' cardiomyopathy. N. Engl. J. Med. 373, 1295–1306. <https://doi.org/10.1056/NEJMoa1507574>.
- Pantaleão, S.Q., Fernandes, P.O., Gonçalves, J.E., Maltarollo, V.G., Honorio, K.M., 2022. Recent advances in the prediction of pharmacokinetics properties in drug design studies: a review. ChemMedChem 17, <https://doi.org/10.1002/cmdc.202100542>.
- Romanelli, M.M., Amaral, M., Thevenard, F., Santa Cruz, L.M., Regasini, L.O., Migotto, A.E., Lago, J.H.G., Tempone, A.G., 2022. Mitochondrial Imbalance of *Trypanosoma cruzi* Induced by the Marine Alkaloid 6-Bromo-2'-de-N-Methylaplysinopsin. ACS Omega 7, 28561–28570. <https://doi.org/10.1021/acsomega.2c03395>.
- Shi, J., Zha, W., 2019. Predicting human pharmacokinetics: physiologically based pharmacokinetic modeling and in silico ADME prediction in early drug discovery. Eur. J. Drug Metab. Pharmacokin. 44, 135–137. <https://doi.org/10.1007/s13318-018-0503-9>.
- Shikanai-Yasuda, M.A., Carvalho, N.B., 2012. Oral transmission of Chagas disease. Clin. Infect. Dis. 54, 845–852. <https://doi.org/10.1093/cid/cir956>.
- Sohlenius-Sternbeck, A.-K., Janson, J., Bylund, J., Baranczewski, P., Breitholtz-Emanuelsson, A., Hu, Y., Tsoi, C., Lindgren, A., Gissberg, O., Bueters, T., Briem,



- S., Juric, S., Johansson, J., Bergh, M., Hoogstraate, J., 2002. Optimizing DMPK properties: experiences from a big pharma DMPK department. *Curr. Drug Metab.* 17, 253–270. <https://doi.org/10.2174/1389200217666151210125637>.
- Tada, H., Shiho, O., Kuroshima, K., Koyama, M., Tsukamoto, K., 1986. An improved colorimetric assay for interleukin 2. *J. Immunol. Methods* 93, 157–165. [https://doi.org/10.1016/0022-1759\(86\)90183-3](https://doi.org/10.1016/0022-1759(86)90183-3).
- Tandon, H., Ranjan, P., Chakraborty, T., Suhag, V., 2021. Polarizability: a promising descriptor to study chemical–biological interactions. *Mol. Divers.* 25, 249–262. <https://doi.org/10.1007/s11030-020-10062-w>.
- Varela, M.T., Romanelli, M.M., Lima, M.L., Borborema, S.E.T., Tempone, A.G., Fernandes, J.P.S., 2018. Antiparasitic activity of new gibbilimol analogues and SAR analysis through efficiency and statistical methods. *Eur. J. Pharm. Sci.* 122, 31–41. <https://doi.org/10.1016/j.ejps.2018.06.023>.
- Varela, M.T., Costa-Silva, T.A., Lago, J.H.G., Tempone, A.G., Fernandes, J.P.S., 2019. Evaluation of the antitrypanosoma activity and SAR study of novel LINS03 derivatives. *Bioorg. Chem.* 89. <https://doi.org/10.1016/j.bioorg.2019.102996>
- Varela, M.T., Amaral, M., Romanelli, M.M., Castro Levatti, E.d., Tempone, A.G., Fernandes, J.P.S., 2022. Optimization of physicochemical properties is a strategy to improve drug-likeness associated with activity: novel active and selective compounds against *Trypanosoma cruzi*. *Eur. J. Pharm. Sci.* 171. <https://doi.org/10.1016/j.ejps.2021.106114> 106114.
- WHO, World Health Organization, 2021. Chagas' Disease Fact Sheet. [https://www.who.int/news-room/fact-sheets/detail/chagas-disease-\(american-trypanosomiasis\)](https://www.who.int/news-room/fact-sheets/detail/chagas-disease-(american-trypanosomiasis)) (accessed 10 March 2023).
- Zhu, B., 2002. Catechol-O-Methyltransferase (COMT)-Mediated methylation metabolism of endogenous bioactive catechols and modulation by endobiotics and xenobiotics: importance in pathophysiology and pathogenesis. *Curr. Drug Metab.* 3, 321–349. <https://doi.org/10.2174/1389200023337586>.